Experimental Test of an Alignment Sensing Scheme for a Gravitational-wave Interferometer

Nergis Mavalvala*, Daniel Sigg† and David Shoemaker

LIGO Project
Department of Physics and Center for Space Research,
Massachusetts Institute of Technology, Cambridge, MA 02139

Submitted to Optics Letters
May 15, 1998

An alignment sensing scheme for all significant angular degrees of freedom of a power-recycled Michelson interferometer with Fabry-Perot cavities in the arms was tested on a table-top interferometer. The response to misalignment of all degrees of freedom was measured at each sensor, and good agreement was found between measured and theoretical values.

KEYWORDS

Gravitational-wave observatories, laser interferometer, automatic alignment, LIGO, Fabry-Perot cavities.

One of the most promising techniques for detecting gravitational waves is through the apparent change in travel time of light along orthogonal axes in the arms of a Michelson interferometer, induced by a passing gravitational wave [1]. To increase their sensitivity, the interferometric gravitational wave detectors currently planned for the Laser Interferometric Gravitational-wave Observatory (LIGO) [2] use resonant Fabry-Perot cavities in each arm of the Michelson interferometer to increase the phase shift of the light returning to the beam splitter and a partially transmitting mirror placed at the input to the interferometer to recycle the light returning toward the laser (see Fig. 1) [3].

In a detector with this optical configuration the two arm cavities and the recycling cavity must be resonant and the path difference of the arms of the Michelson interferometer must result in nearly perfect destructive interference. Currently planned interferometers use extensions of a heterodyne phase sensing technique often referred to as Pound-Drever-Hall reflection-locking [4], [5] to detect longitudinal deviations from resonance. In its simplest form (applied to a simple Fabry-Perot cavity), phase modulation sidebands outside the cavity linewidth are imposed on the incident laser light and deviations in cavity length which detune the carrier resonance induce an intensity modulation at the sideband frequency in reflected light proportional to length deviations which can be used in a feedback loop to keep the cavity on resonance.

An important mechanism by which the sensitivity of this resonant optical system can be degraded is angular misalignment of the interferometer mirrors with respect to the incoming laser beam. Misalignment reduces the gravitational wave sensitivity either by allowing unwanted light power to leak out of the antisymmetric Michelson port, which increases the shot noise; or by lowering

the stored light power in the arm cavities, thereby decreasing the signal induced by a gravitational wave. Consequently, to achieve maximum gravitational wave strain sensitivity the absolute angle of each mirror relative to the incoming laser beam must be less than 10^{-8} radians r.m.s. [6].

Since the modes of a misaligned resonant cavity have a different spatial profile from that of the incident beam, the spatial pattern of the fields reflected from the cavity carries information about the alignment state of the cavity. The measurement of angular misalignments in a resonant optical cavity by heterodyne detection of off-axis spatial modes was first proposed and demonstrated by Anderson and Sampas [7]. Morrison et al. [8] adapted the Pound-Drever-Hall technique by using the spatial asymmetries of the amplitude modulated light reflected from the cavity to detect angular misalignment of the cavity mirrors with respect to the incoming laser beam. Signals proportional to length deviations are obtained by detecting the total reflected light power, while alignment signals are determined by taking the difference of opposing halves of a split photodetector. A significant advantage of this method is that if the cavity length is held on resonance for the carrier light frequency using the Pound-Drever-Hall reflection locking technique no additional sidebands are required to sense the deviations from perfect alignment. An important — and useful — difference between length and alignment sensing is the presence of axial or Guoy phase shifts acquired by higher-order transverse modes due to free space propagation [9]. Alignment signals due to misalignment of the input or rear mirror of the resonant cavity are thus distinguishable due to their relative phase shift.

An alignment sensing scheme for a two-mirror resonant cavity is comprised of two quadrant photodetectors placed at specific distances from the input mirror, corresponding to the optimal Guoy phase shift for detection of input and rear mirror misalignments. The signal from each quadrant is demodulated at the modulation frequency and the difference of two opposite pairs of quadrants is proportional to misalignment of the particular degree of freedom. Conveniently, the sum of all four quadrants gives the length sensing signal. We refer to the quadrant photodetector and its associated electronics as a *wavefront sensor.*

Similarly, in a complex optical system such as the power-recycled interferometer used for gravitational wave detection, an unambiguous signal for each length and alignment degree of freedom can be obtained. Numerous signal extraction schemes for sensing deviations from perfect longitudinal interference, based on a combination of suppressed carrier and Pound-Drever-Hall reflection locking techniques, have been developed and tested [10], [11]. The signals for the four longitudinal degrees of freedom are sensed at one or more of three detection ports — or outputs — of the interferometer: the anti-symmetric port, the reflection port and the recycling cavity pick-off port (see Fig. 1). Analogous to the simple cavity, alignment signals can be derived by spatially sampling the fields at the detection ports. Alignment signals are extracted using the above heterodyne phase detection techniques; the magnitude of angular misalignments is measured by detecting the spatial gradients in the interfering carrier and sideband fields.

Distinct discriminants for ten angular degrees of freedom can be derived by judicious placement of five wavefront sensors at three detection ports. Most generally, the signal detected by the *i*-th wavefront sensor is

$$WFS_i \propto \sum_j A_{ij}\Theta_j \cos(\eta_i - \eta_{ij}) \cos(\Omega_i t - \phi_{ij}) \qquad (1)$$

where the sum is taken over all *j* angular degrees of freedom. Θ_j is the misalignment angle of the *j*-th degree of freedom, η_i is the Guoy phase shift between the detection port and the detector, η_{ij} is the intrinsic Guoy phase shift of the signal, Ω_i is the modulation frequency and ϕ_{ij} is the intrinsic RF phase shift of the signal. The elements of the alignment sensitivity matrix, A_{ij}, depend on the optical parameters of the interferometer and on the particular signal extraction scheme used.

The alignment sensing scheme used in the table-top experiment [12] is based on a multiple-carrier signal extraction scheme [11]. A schematic representation of the experiment is shown in Fig. 1. Interference between a main carrier, which is resonant in the arm cavities and the recycling cavity, and a pair of phase modulation sidebands resonant only in the recycling cavity is used to extract both length and alignment signals for the arm cavities. Differential misalignments of the arm cavity mirrors, like differential length deviations, are detected primarily at the antisymmetric port (WFS_4). Similarly common-mode misalignments of the arm cavity mirrors are sensed at either the reflection port (WFS_5) or at the recycling cavity pick-off port (WFS_6), as are the common-mode length deviations. A frequency-shifted subcarrier and a pair of phase modulation sidebands, all of which resonate in the recycling cavity but not in the arm cavities, are used to detect differential misalignments of the arm cavity input mirrors at the anti-symmetric port (WFS_3). An additional pair of subcarrier sidebands, which are not resonant anywhere in the interferometer are used to sense common-mode misalignments of the arm cavity input mirrors and the power-recycling mirror at the reflection port (WFS_1 and WFS_2). Since the subcarrier is anti-resonant in the arm cavities, signals derived from the subcarrier and its sidebands are most sensitive to the Michelson degrees of freedom and nearly independent of arm cavity deviations. The resulting alignment sensitivity matrix, *A*, is non-singular, which makes it possible to clearly separate individual mirror angles.

The matrix elements of *A* were calculated using a model based on mode decomposition of the interferometer fields [13] and inverted to give coefficients for a low frequency (1 Hz) digital feedback system to bring the resonant interferometer into an optimal alignment state. To measure experimentally the alignment sensitivity matrix elements, each angular degree of freedom was dithered at a distinct frequency well above the bandwidth of the angular servos; signals from the wavefront sensors and from a set of optical levers, one for each mirror, were analyzed off-line. The Fourier transforms of the measured time series for each optical lever and each wavefront sensor were computed. By determining the signal amplitude due to each angular degree of freedom in each wavefront sensor and optical lever spectrum and by taking into account the light power hitting the wavefront sensors, their quantum efficiency and their transimpedance gain, we directly calculated each element of the alignment sensitivity matrix.

In Fig. 2 we plot the experimentally determined matrix elements against the values predicted by the mode decomposition model. Since the matrix elements which are predicted to be very small do indeed correspond to insignificant signals on the wavefront sensors, only the dominant elements of the alignment sensitivity matrix, averaged over horizontal and vertical degrees of freedom, are shown. The error bars arise from uncertainties in the power built up in the recycling cavity (6% – 24%, depending on the matrix element), the Guoy phase shift in the telescopes (~1% for on-diagonal elements and 5% – 20% for off-diagonal elements), the transimpedance gains of the wavefront sensors (5% –10%), the absolute light power incident on each detector (6%), the modulation indices (5% – 10%) and the calibration of the pointing system (10%). The statistical uncertainties are small, typically below 3%. Since these uncertainties are independent of each

other they are added in quadrature, resulting in about ±20% total uncertainty for the matrix elements plotted in Fig. 2.

The quantitative agreement between the modal model predictions and the measurement, evinced in Fig. 2, is a strong validation of the model. It gives us confidence that a complete set of alignment signals can be experimentally determined in a complex resonant optical system with sufficient precision to enable a precision alignment sensor. Based on the wavefront sensing scheme, we have designed an automatic alignment system for LIGO [6]. We conclude that the wavefront sensing technique is well understood, both theoretically and experimentally, and that this technique is feasible for closed loop servo control of complex resonant optical interferometers.

We thank our colleagues on the LIGO project who helped us carry out this experiment and gave us many useful suggestions and comments, particularly R. Weiss and S. Whitcomb. Most of all, we thank Y. Hefetz, who initiated this experiment and much of the analysis preceding it. This work is supported by NSF grant PHY-9210038. One of us (D. Sigg) was partially supported by the Swiss National Science Foundation.

* Present address, Physics Department, California Institute of Technology, Pasadena, California 91125.

† Present address, LIGO Project, P.O. Box 1970, M.S. S9-02, Richland, Washington 99352.

REFERENCES

[1] R. Weiss, MIT Res. Lab. Electron. Q. Prog. Rep. **105**, 54 (1972).

[2] A. Abramovici, W. E. Althouse, R. W. P. Drever, Y. Gürsel, S. Kawamura, F. J. Raab, D. Shoemaker, L. Sievers, R. E. Spero, K. S. Thorne, R. E. Vogt, R. Weiss, S. E. Whitcomb and M. E. Zucker, Science **256**, 325 (1992).

[3] See, for example, R. W. P. Drever, "Interferometric Detectors for Gravitational Radiation," in *Gravitational Radiation*, N. Deruelle and T. Piran, eds. (North Holland Publishing, Dordrecht, 1983), pp. 321–338.

[4] A. Schenzle, R. DeVoe and G. Brewer, Phys. Rev. A **25**, 2606 (1982).

[5] R. W. P. Drever, J. L. Hall, F. V. Kowalski, J. Hough, G. M. Ford, A. J. Munley and H. Ward, Appl. Phys. B **31**, 97 (1983).

[6] P. Fritschel, G. González, N. Mavalvala, D. Shoemaker, D. Sigg, and M. Zucker, *submitted to Applied Optics* (1998).

[7] D. Z. Anderson, Appl. Opt. **23**, 2944 (1984); N. Sampas and D. Z. Anderson, Appl. Opt. **29**, 394 (1990).

[8] E. Morrison, B. J. Meers, D. I. Robertson, and H. Ward, Appl. Opt. **33**, p. 5037 (1994); E. Morrison, B. J. Meers, D. I. Robertson, and H. Ward, Appl. Opt. **33**, 5041 (1994).

[9] A. E. Siegman, *Lasers* (University Science, California, 1986) p. 682—685.

[10] M. W. Regehr, F. J. Raab, and S. E. Whitcomb, Opt. Lett. **20**, 1507 (1995).

[11] D. Sigg, N. Mavalvala, J. Giaime, P. Fritschel, and D. Shoemaker, *accepted for publication in Applied Optics* (1998).

[12] N. Mavalvala, "Alignment Issues in Laser Interferometric Gravitational-wave Detectors," Ph. D. dissertation (Massachusetts Institute of Technology, Cambridge, Mass., 1997)

[13] Y. Hefetz, N. Mavalvala, and D. Sigg, J. Opt. Soc. Am. B **14**, 1597 (1997).

FIGURE CAPTIONS

Figure 1: Overview of the experiment. The length sensors and wavefront sensors (WFS_i) are placed at three signal detection ports. A pellicle beam splitter is used to pick off a tiny fraction of the light inside the power recycling cavity.

Figure 2: Dominant elements of the alignment sensitivity matrix compared with the values predicted by the model. Calculated values are along the horizontal axis and the vertical axis corresponds to measured values (all values are given in arbitrary units). Each wavefront sensor is designated by a different symbol; the error bars are explained in the text.

FIGURES

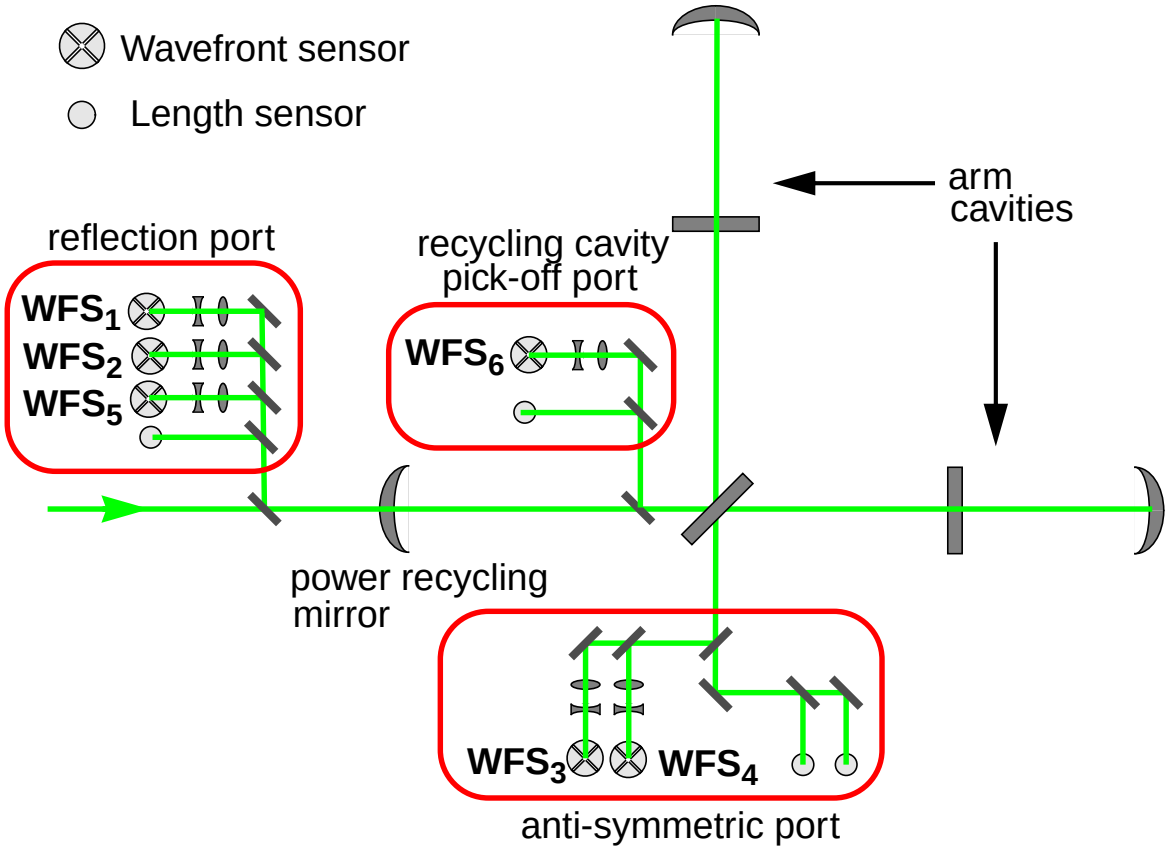

Figure 1 Mavalvala

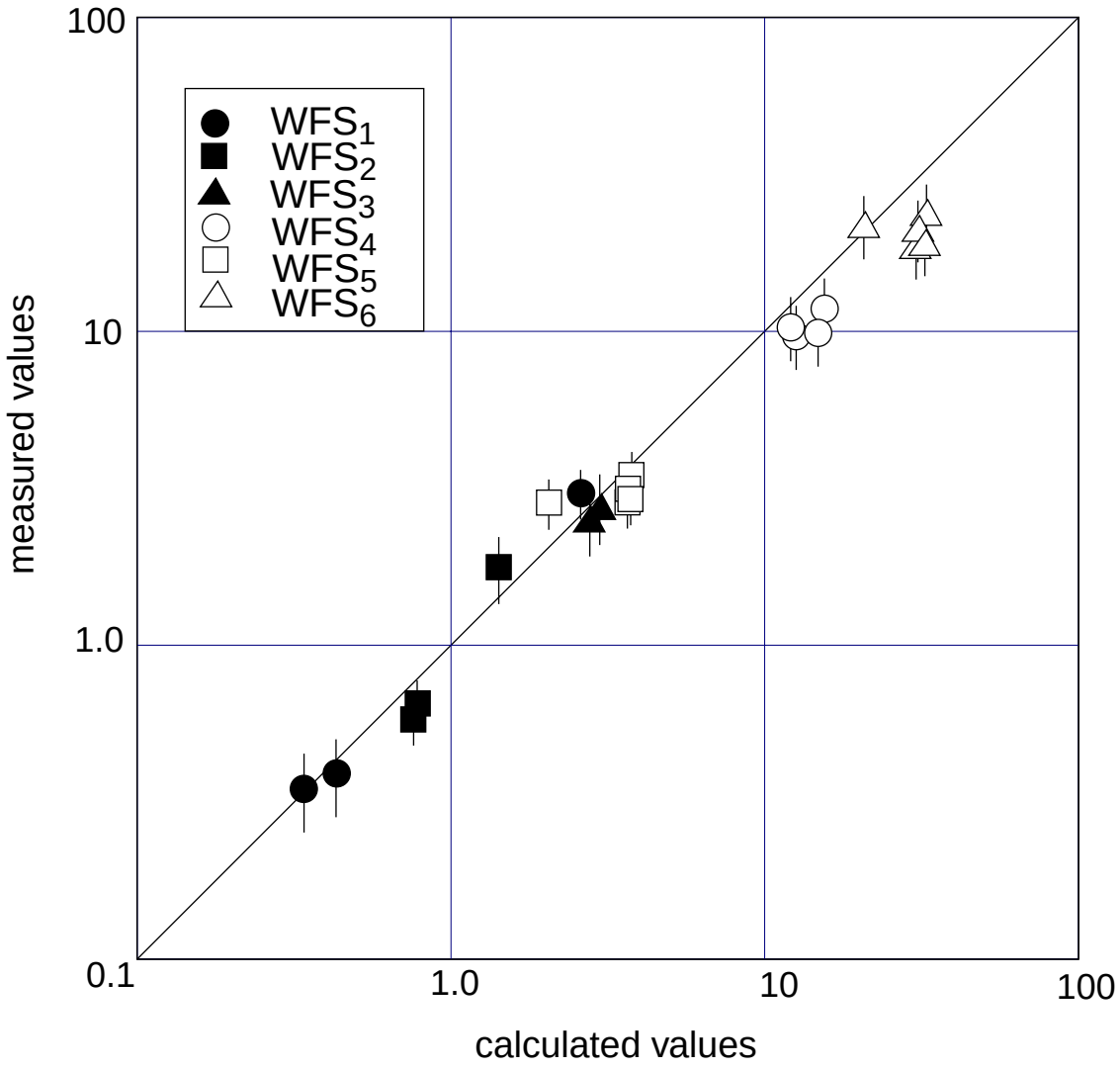

Figure 2

Mavalvala